Nuclear Inst, and Methods in Physics Research B 420 (2018) 69–75

Contents lists available at ScienceDirect

Nuclear Inst. and Methods in Physics Research B

journal homepage: www.elsevier.com/locate/nimb

Dependence of yield of nuclear track-biosensors on track radius and analyte concentration

H. García-Arellano[a], G. Muñoz H.[b], D. Fink[b,c,*], J. Vacik[c], V. Hnatowicz[c], L. Alfonta[d], A. Kiv[e]

[a] Departamento de Ciencias Ambientales, División de Ciencias Biológicas y de la Salud, Universidad Autónoma Metropolitana-Lerma, Av. de las Garzas No. 10, Col. El Panteón, Lerma de Villada, Municipio de Lerma, Estado de México C. P. 52005, Mexico
[b] Departamento de Fisica, Universidad Autónoma Metropolitana-Iztapalapa, PO Box 55-534, 09340 México, D.F., Mexico
[c] Nuclear Physics Institute, ASCR, 25068 Řež, Czech Republic
[d] Department of Life Sciences and Ilse Katz Institute for Nanoscale Science and Technology, Ben-Gurion University of the Negev, PO Box 653, Beer-Sheva 84105, Israel
[e] Ben-Gurion University of the Negev, PO Box 653, Beer-Sheva 84105, Israel

ARTICLE INFO

Keywords:
Biosensor
Ion track
Etching
Enzyme
Nanofluidics

ABSTRACT

In swift heavy ion track-based polymeric biosensor foils with incorporated enzymes one exploits the correlation between the analyte concentration and the sensor current, via the enrichment of charged enzymatic reaction products in the track's confinement. Here we study the influence of the etched track radius on the biosensor's efficiency. These sensors are analyte-specific only if both the track radii and the analyte concentration exceed certain threshold values of ~15 nm and $\sim 10^{-6}$ M (for glucose sensing), respectively. Below these limits the sensor signal stems un-specifically from any charge carrier. In its proper working regime, the inner track walls are smoothly covered by enzymes and the efficiency is practically radius independent. Theory shows that the measured current should be slightly sub-proportional to the analyte concentration; the measurements roughly reconfirm this. Narrower tracks (~5–15 nm radius) with reduced enzyme coverage lead to decreasing efficiency. Tiny signals visible when the tracks are etched to effective radii between 0 and ~5 nm are tentatively ascribed to enzymes bonded to surface-near nano-cracks in the polymer foil, resulting from its degradation due to aging, rather than to the tracks. Precondition for this study was the accurate determination of the etched track radii, which is possible only by a nanofluidic approach. This holds to some extent even for enzyme-covered tracks, though in this case most of the wall charges are compensated by enzyme bonding.

1. Introduction: Going to the sensor's limits

Since a few decades latent and etched ion tracks in thin polymer foils [1,2] are applied for biosensing [3]. From the different measuring strategies, we favour the "Product Enhancement" strategy [3] most. Here, enzymes are fixed to the walls of transparent etched ion tracks in a polymer foil. Whenever analyte molecules enter, the enzymes digest them towards the corresponding characteristic reaction products. If the product's formation speed is higher than their escape speed from the tracks, they will enrich within the tracks [4]. This is given whenever the analyte concentration is not too low and whenever the etched track's aspect ratio l/r (l = track length, r = track radius) is sufficiently large. The latter case is fulfilled for conventional etched ion tracks in polymers such as polyethylene terephthalate (PET), which have typical aspect ratios (i.e., length/diameter ratios) of up to ~1000 or so. The higher the product accumulation within the tracks is,[1] the larger is the biosensing signal [4]. Basic pre-condition for this sensing technique is that both the analyte and the enzymatic reaction products differ in their charge states[2] from each other, so that changes in the track conductivity reveal the presence of the analyte.

Hitherto, this technique has been applied by us for sensing of glucose (via the enzyme glucose oxidase, GOx) [5], urea (via the enzyme urease) [6] and phenols (via the enzyme laccase) [7]. The "Product Enhancement" strategy is advantageous due to the ease of production (no facility for single ion track production necessary), a wide tolerance for sensor operation (concerning the etched track fluences and radii), relatively large sensor currents (due to the simultaneous use of up to $\sim 10^9$ tracks/cm^2 in a foil), its environmental friendliness (only

* Corresponding author.
E-mail address: fink@xanum.uam.mx (D. Fink).

[1] The product accumulation can be enhanced b, g., long track lengths, narrow track diameters, a high ratio between the analyte's to the product's diffusion coefficients or by the closure of one track opening [4].

[2] See, e.g., the case of glucose sensing with glucose oxidase, where the analyte glucose is neutral and the product gluconic acid is ionized; hence the enzymatic reaction leads to an increase in the charge state of the liquid in the etched in tracks.

https://doi.org/10.1016/j.nimb.2018.02.010
Received 2 May 2017; Received in revised form 22 January 2018; Accepted 8 February 2018
Available online 14 February 2018
0168-583X/

polymers and enzymes are required), its low cost (only ~ng of enzymes are used), its possibility for manyfold sensor re-use (at least some ~30 times), the robustness of the sensors against thermal denaturation (storing them outside the fridge for several days hardly has any negative influence on their performance) and the prolonged sensor lifetimes (up to ~3 months or more are possible if stored in a fridge).

In the view of the success of this strategy we thought it worthwhile to test its utmost limits of applicability. We were especially interested in finding out what happens when steadily reducing both the analyte concentration and the etched track diameter (hence also rising the track aspect ratio). Two questions arose in this connection, namely a) how does nanofluidics influence the sensor's behaviour and b) does the enzyme's reaction kinetics influence the sensor's detection sensitivity?

2. Experimental

2.1. Details of sensor preparation

For our biosensor experiments, we applied PET (Melinex and Hostaphan) and polycarbonate (Makrofol KG) foils (denoted here as foils #6, #8 and #15 for consistency with recent track etching studies in Ref. [8]). Though these foils are already 20, 4 and 6 years old, respectively, they all still maintain good plasticity and etchability and therefore are feasible for biosensor production. These foils were irradiated by energetic heavy ions to create straight parallel radiation-damaged regions ('latent ion tracks') therein. For this publication, we mostly used foil #8 with the following specifications: thickness 19 μm, irradiated by 170 MeV Xe ions up to a fluence of 1×10^7 cm^{-2}. The less frequently used foil #6 is 12 μm thick and was irradiated by 250 MeV Kr ions up to a fluence of $4 \times 10^6\,cm^{-2}$, Finally, foil #15 is 8 μm thick and was irradiated by 985 MeV Au ions up to a fluence of $2 \times 10^8\,cm^{-2}$. The samples, cut to typical sizes of $\sim 1 \times 1\,cm^2$, were etched with 4 M NaOH at room temperature (~22C) in a specially designed etching chamber (which was made after the example of Ref. [9]). The etching procedure was constantly monitored by conductometry, applying for this purpose a power supply (inner resistance: $R_{int} = 1\,M\Omega$) which delivered a sinusoidal voltage of ~2 V at ~50 mHz. The transmitted currents were measured with an oscilloscope (inner resistance $R_o = 1\,M\Omega$) with a measuring point resistance R_s which could take values of 0 and 9 MΩ, depending on the measuring task [8].

During the etching the radiation-damaged material along the latent ion tracks was preferentially dissolved and removed, thus transforming the latent ion tracks into "etched tracks". As in this transition region we observe a gradual opening and merging of the radiation-induced free volume zones towards narrow nanopores, these tiny structures are by no means all of perfectly conical or cylindrical shape, but instead exhibit individual statistical variations. This means that the track radii r derived here must be considered as "effective radii" only, i.e., they are mean values, averaged over the whole track lengths, and they do not give any clue for the accurate track shapes. For this work, we prepared etched tracks of cylindrical (in the track core region for radii < 10 nm) or funnel-type shapes (for larger tracks) [2,8,10]).

After etching to appropriate track diameters (as measured after replacing the etchant by ultrapure water and calculating the radius from the transmitted current), the foils were washed with activation buffer (0.1 M MES (2-[morpholino]ethanesulfonic acid), 0.5 M NaCl, pH 6.0) and immersed in a solution of 2 mM 1-ethyl-3-[3-dimethylaminopropyl]carbodiimide (EDC) and 5 mM *N*-hydroxysulfosuccinimide (S-NHS) for 15 min. The activated foils were then washed with coupling buffer (0.1 M sodium phosphate, 0.15 M NaCl, pH 7.2) and immersed into a solution of 10 mg/mL glucose oxidase (GOx). After 2 h, the foils were rinsed extensively with phosphate buffer to eliminate the non-bonded GOX and stored at 4 °C in phosphate buffer until use. For reliable comparison of the sensors with each other, we treated all of them in exactly the same way, independent of their individual etched track size. Immediately before starting with the measurements, the biosensor foils were accommodated to the new ambient, by either washing them typically 10 times or so with ultrapure water (supplier: Millipore Corp. (Merck), conductivity $18.2\,M\Omega^{-1}\,cm^{-1}$) until their conductivity remained constant, or by allowing them to release their buffer ions for at least ~40 min in ultrapure water, with roughly the same result, Fig. 1. Thereafter the sensors were ready for use with the utmost possible measuring sensitivity.

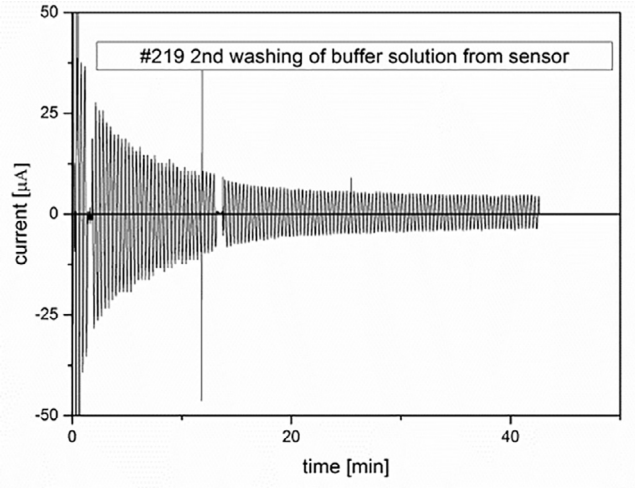

Fig. 1. Accommodation of biosensor #219, (made of foil #6, side B [8]) from storage in buffer solution to the measurement in ultrapure water, as described by the transmitted current as a function of accommodation time. In this case, we both allowed the buffer ions to diffuse out from the sensor foil into the ultrapure water ambient by just waiting, and also changed the ambient solution two times (see the interruptions). No remarkable difference shows up during either waiting for an hour or so, or during changing the washing water multiple times. Sinusoidal alternating voltage of 5 V, 49.5 mHz applied; measurement with oscillscope; no shunt used.

2.2. Derivation of the etched track radii from measured transmitted test currents

Until recently, it is convenient to calculate the etched track radii from test currents transmitted through them by conventional macroscopic conductometry [2,10,11]. However, meanwhile it is known that macroscopic flow conditions break down in nanopores and have to be replaced by a nanofluidic approach (see eg., the excellent recent review article by Bocquet et al. [12], or others [13–15]). As to our knowledge, the nanofluidic conversion from conductometrically determined test currents across etched tracks to nanopore radii has not yet been explicitly reported,[3] we care for it here. To follow this procedure, the knowledge of both the ionic conductivity in the nanopore K_{Bulk} and the density of the charges $K_{Surface}$ on the nanopore surfaces is essential.

Scaling Bocquet's numerical example of a representative monovalent nanofluidic system [12] down to our *as-etched* and subsequently water-filled tracks (i.e., before any enzyme deposition starts), then $K_{Bulk} \sim 5.5 \times 10^{-8}\,Scm^{-1}$ (corresponding to the impurities in ultrapure water, estimated to be in the order of $C_{Bulk} \sim 10^{-7}$ M) and $K_{Surface} \approx 0.1\,e/nm^2 = 1.6\,\mu C/cm^2$ are applicable. Then, the system's characteristic nanofluidic lengths are: the Bjerrum length: $l_B = 0.7$ nm (for whatever K_{Bulk} and $K_{Surface}$), the Debye length: $\lambda_D \sim 0.9$ μm and the Dukhin length: $l_{DU} \sim 1.6$ mm. Scaling, however, these results down to enzyme-covered *biosensor* tracks (where surface charges are largely neutralized due to enzyme bonding), we should rather assume $C_{Bulk} \sim \{10^{-7}$ to $10^{-6}\}$ M (hence $K_{Bulk} < 5.5x10^{-7}\,Scm^{-1}$) and $K_{Surface}$

[3] Possibly this stems from the researcher's (perhaps intentional) selection of high salt concentrations, specific pH values, and low voltages for track radius calculations, which reduces the nanofluidic influence considerably and avoids the otherwise necessary lengthy calculations.

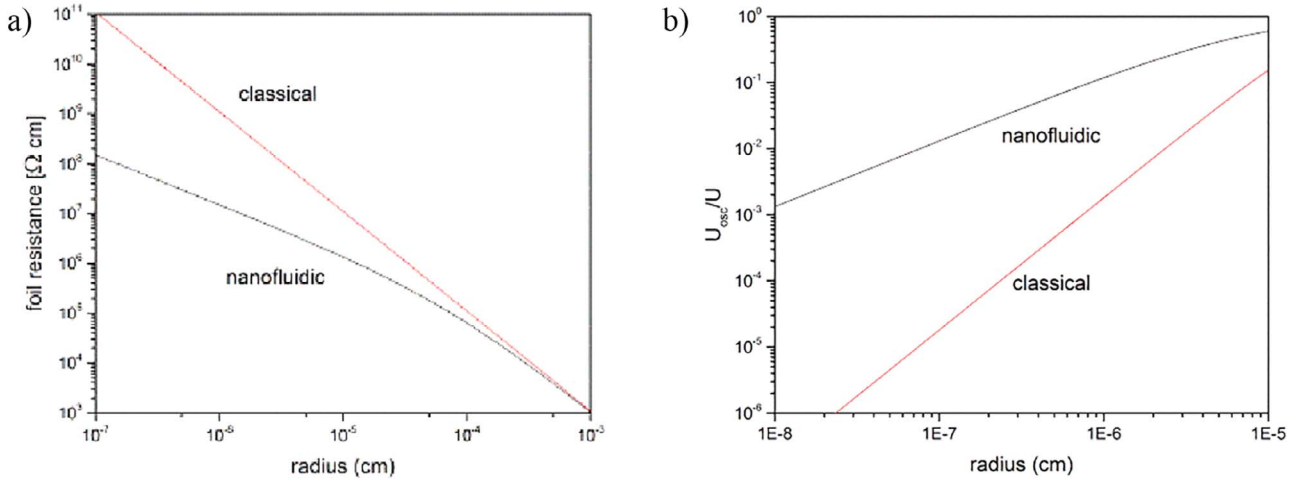

Fig. 2. Application of nanofluidic theory to the experimental case treated here (Foil # 8) for the as-etched polymer foil's current transmission measurement after immersion in ultrapure ("milliQ") water), to a) the resistances of our etched foils and b) the measured oscilloscope voltages (normalized to the applied voltage U) in dependence of the etched track radii; detail of the most interesting range region. Chosen values: $K_{Bulk} = 5.5 \times 10^{-8}$ Scm^{-1} (corresponding to 10^{-7} M) and $K_{Surface} = 1.6$ μC/cm^2. Both the results obtained with conventional macroscopic physics ("classical") and with nanofluidics are shown.

~1.6 nC/cm^2, so that we arrive at estimates of $l_B = 0.7$ nm, λ_D ~0.3 μm (max. ~1 μm) and l_{DU} ~1.6 μm (max. ~16 μm), respectively (the numbers in brackets describe the possible most active biosensor states).

The large sizes of the Dukhin length mean that here, surface charges play a significant role, though after their reduction by enzyme bonding the nanofluidic influence is reduced considerably. With the above data base, it is possible to calculate the electric conductance G_p (i.e., the ratio of transmitted electric current I versus the electrical potential drop E_e) of a nanopore as the sum of both the its central and surface contributions according to [16–19], and consequently also the resistance of all Φ nanopores per unit area [12,17–20], from which finally the etched track radii can be determined. Due to the negligible surface charges of our biosensors, perturbations by three-dimensional streamlines outside the nanopores as predicted by Lee et al. [20] (which would make the track openings appear larger than they are in reality) vanish in our case.

The final correlations between the foil resistances and the *as-etched* track radii (i.e., *before* enzyme deposition onto the corresponding track walls) are depicted in Fig. 2a, as well for the classical macroscopic, as also for the nanofluidic approaches. The same is done for the correlations between the measured oscilloscope voltages U_{osc} in our measuring chamber and the etched track radii, see Fig. 2b. As expected, the nanofluidic influence of surface currents during narrow track etching is considerable, leading to corrections of more than an order of magnitude for the as-etched tracks. This applies especially for ion track cores and their transition regions to the penumbra.

For the *final* biosensors (i.e., *enzyme-clad* etched tracks with near-zero surface charge), Fig. 3 gives the corresponding curves for a, b) their overall electrical resistances and c) the measured oscilloscope voltages U_{osc} as a function of the track radii. As we had obtained above only rough estimates for both the ionic conductivity K_{Bulk} and the surface charge density $K_{surface}$ of our biosensors (that also depends on later modification steps), we give here a bunch of curves for different values around the expected ones (which indicates the magnitude of error of this calculation). It is seen that for surface charges below ~1 nC/cm^2, nanofluidic surface currents become negligible. It further follows that under the experimental circumstances given here, the *maximum* radius of track-based biosensors which can be recorded[4] with reasonable accuracy when using ultrapure (milliQ) water is in the order of a few hundred nm.

A remark: in literature it is commonly assumed that the smallest tracks which can be reasonably produced by etching, and also which can be reasonably detected by conductometry, are in the range of several nm only [2]. This conclusion was hitherto always based on the classical current-to-radius conversion. However, as illustrated by e.g., Fig. 2a, an ultrapure water-filled track for which a resistance of, let us say, 10^8 Ωcm was measured and to which a radius of ~2×10^{-6} cm would be assigned conventionally, would obtain a radius of only ~1×10^{-7} cm if evaluated nanofluidically. It is this difference by more than an order of magnitude which makes the track radii appear here unusually narrow. The narrowest radius obtained by us conventionally, ~15 nm, would then turn to ~0.3 nm if calculated nanofluidically. According to our previous remark, we denote these calculated results only as "effective track radii" as it is doubtful in how far such narrow radii are still realistic.

3. Results and discussion

3.1. The effective enzyme layer thickness

We now determine the differences $dr = r_{etch} - r_{sensor}$ between the measured as-etched track radii r_{etch} and the radii of the biosensors r_{sensor} produced from these etched tracks, as a function of r_{etch}, for as well the classical macroscopic approach as according to nanofluidics, see Fig. 4. In the latter case, we used for the evaluation of r_{etch} the most appropriate parameters $K_{Bulk} = 5.5 \times 10^{-8}$ Scm^{-1} (corresponding to ~10^{-7} M) and $K_{Surface} = 1.6$ μC/cm^2. For the evaluation of the biosensor track radii r_{sensor} we used a K_{Bulk} value of 5.5×10^{-7} Scm^{-1} and a $K_{Surface}$ value of 1.6 nC/cm^2.

What one would expect is that this difference dr is always constant, as both the as-etched and enzyme-clad tracks just differ by the deposited enzyme layer, its thickness being given by the enzyme diameter d_{enzyme}. However, Fig. 4 shows strong differences for both the classical and the nanofluidic evaluation: though these differences are constant within an interval B, they become negative for too small r_{etch} (interval A), and they grow steadily for very large r_{etch} (interval C). Therefore we denote these differences dr as the "effective enzyme layer thickness".

The comparison between Fig. 4a and b indicates that the nanofluidic

[4] Larger track radii can only be measured after changing the experimental parameters such as reducing the sample foil size by at least a factor ~3, or the electrolyte conductivity (by "diluting" the used ultrapure water ions with e.g. concentrated sucrose solution [as the latter is neutral and does not react with GOx if present], thus reducing its conductivity by one or more orders of magnitude).

(*footnote continued*)

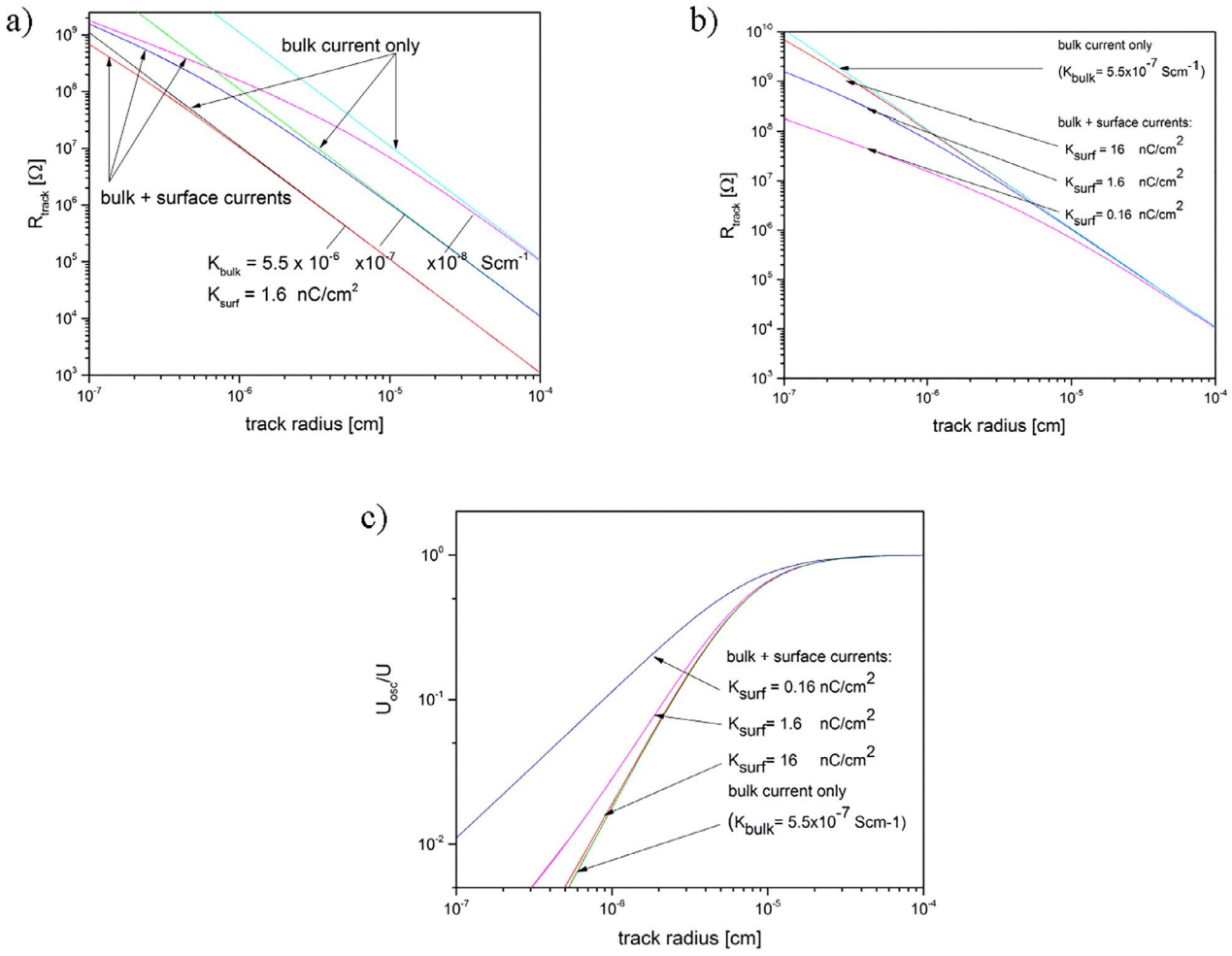

Fig. 3. Application of the above theory to the experimental case treated here (enzyme-clad foil # 8, embedded into ultrapure ("milliQ") water), to a, b) the resistances of our biosensor foils and c) the measured oscilloscope voltages (normalized to the applied voltage) in dependence of the etched track radii. Due to the uncertainty of our estimated K_{bulk} and $K_{Surface}$ values, we give here a bunch of curves for different (a) K_{Bulk} and (b) $K_{Surface}$ values. We think that $K_{Surface}$ values around ~1 nC/cm^2 may be most realistic. K_{bulk} ~5.5×10^{-8} Scm^{-1} may be a good description for sensors at rest or operating at very low analyte concentrations, and K_{bulk} ~5.5×10^{-7} Scm^{-1} may describe better sensors under high analyte load after prolonged times.

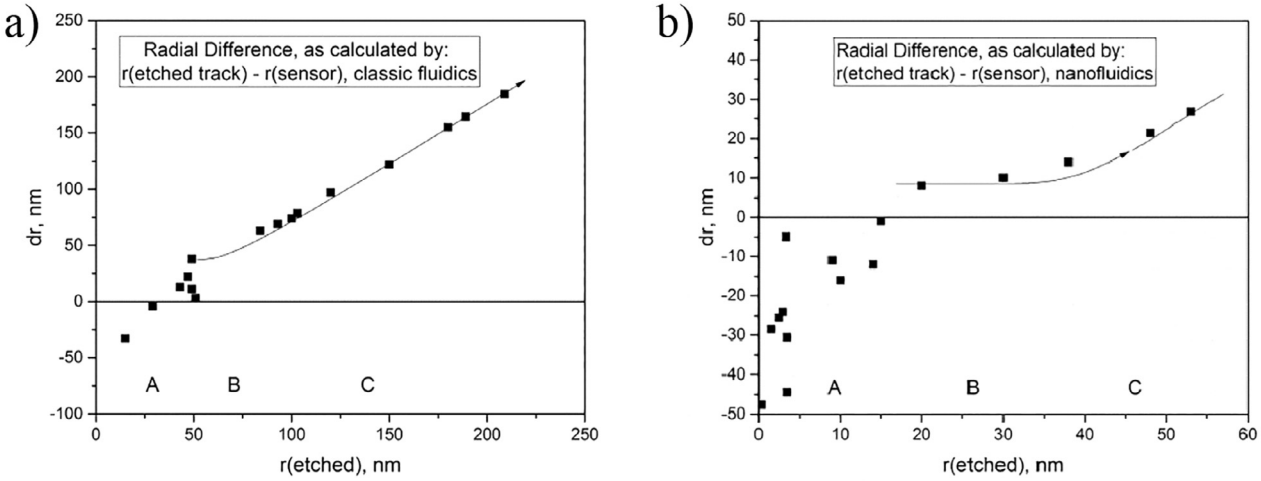

Fig. 4. Effective enzyme layer thickness on the etched track walls, as calculated from the differences of as-etched track radii and radii of etched tracks clad with enzymes (in some cases, the measurements were repeated, to obtain better statistics). Evaluation for a) the classical macroscopic, and b) the nanofluidic model. The letters A, B and C refer to the different regimes found in these plots which describe (A) too narrow etched tracks which cannot yet accommodate enzymes, and (B, C) sufficiently large etched tracks of cylindrical shape which accommodate enzymes on their inner surfaces. C denotes the track regime where dr is no longer constant. Lines to guide the eye.

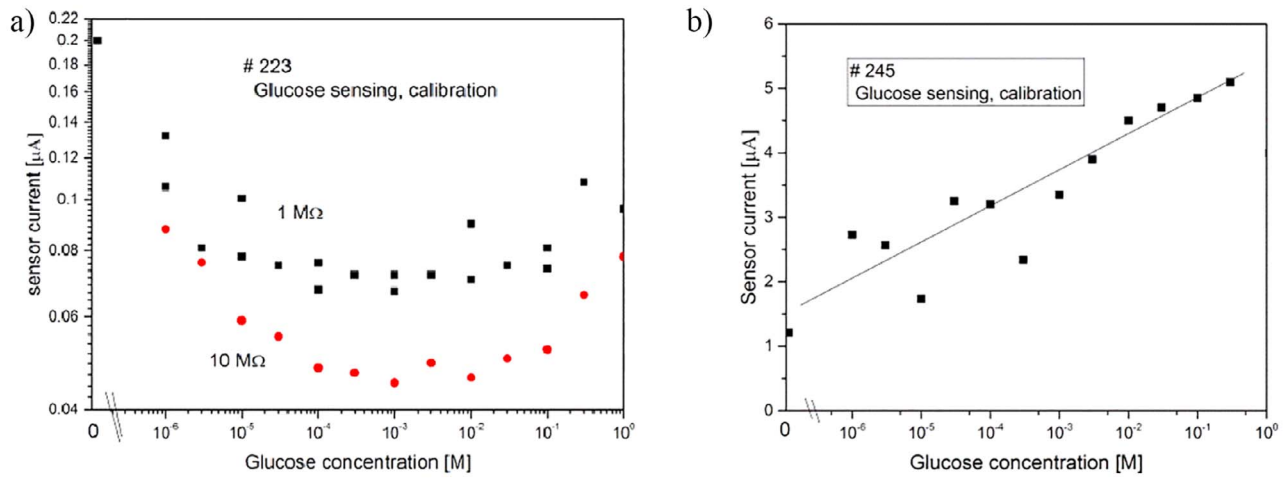

Fig. 5. Two representative examples of glucose sensor calibration curves, for a) sensors with effective radii below the ion track core size and b) a sensor with radius corresponding to the ion track penumbra region. In detail: a) sensor #223 (from foil #6); effective etched track radius ~0.3 nm, b) sensor #245 (from foil #15; track radius 15 nm (as calculated nanofluidically). a) measured with different oscilloscope tip resistances 1 and 10 MΩ, b) measured only with tip resistance 1 MΩ.

evaluation yields a much more realistic picture than the classical approach: Whereas the range interval of region B (with constant dr) is negligibly narrow for the classical approach, it ranges from at least r_{etched} ~16 to 35 nm according to nanofluidics. Further, unrealistically high values emerge for dr in the macroscop approach, whereas the nanofluidic value dr ~8 nm corresponds exactly to the known diameter d_{enzyme} of the deposited enzyme. Therefore we discard from now on the macroscopic calculation and restrict to the nanofluidic picture only.

The strong decrease of dr below r_{etch} = 16 nm indicates that the etched tracks require a radius of at least 16 nm (= 2 d_{enzyme}) to allow the enzyme molecules to smoothly pass each other for the formation of a proper enzyme layer. This is amazing insofar as simple geometric considerations would rather suggest that GOx transport along the tracks starts when $r_{etch} > d_{enzyme}/2$, i.e. that radii around ~5 nm could already be sufficient. Therefore we speculate that for track radii between ~5 and 16 nm (region A), at least some GOx molecules might still be capable to enter the tracks and sporadically cover the track walls, so that some reduced sensor activity may still survive in these cases. In fact, we will show below that this idea does make sense as it is reconfirmed by the growth of the sensor signal in Fig. 6 between r_{etch} = 5–15 nm. For r_{etch} below ~5 nm, geometrical considerations would not allow any more enzyme entering the tracks.

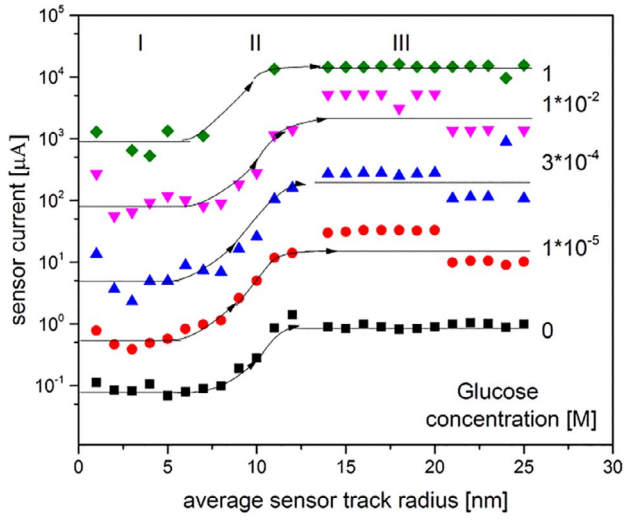

Fig. 6. The recorded sensor current as a function of r_{sensor} (as determined according to the nanofluidic calibration for as-etched tracks after enzyme deposition), for all examined samples, at different applied glucose concentrations, For the sake of clearness, all curves are shifted from each other by a factor 10 in the sensor current scale. Lines to guide the eye.

In the cases where the track surfaces are no longer fully covered with enzymes, the pores do not lose their surface charges any longer, so that here the full nanofluidic mechanism of as-etched tracks applies. Consequently, in this region the low *biosensor*'s charge density values will turn to the higher *as-etched* track's $K_{Surface}$ values in the evaluation (this is not yet done in Fig. 4). Doing this, the r_{sensor} values as evaluated for the biosensor case will decrease towards r_{etch} of the as-etched tracks; hence $dr = r_{etch} - r_{sensor} \rightarrow r_{etch} - r_{etch} = 0$. So the seeming problem of negative enzyme layer thicknesses evidently vanishes.

In conclusion: a) The lowest possible etched track radius which allows for *full* accommodation of enzyme cover layers on the etched track walls is in the order of $2d_{enzyme,}$ here: 16 nm. b) In some transition regime (above ~5 nm radius) limited biosensing is still possible, due to the arrival of a few enzyme molecules in this highly confined region. c) Smaller etched tracks are useless for biosensor production. d) The puzzling negative dr values of Fig. 4 are artefacts arising from the inadequate choice of the type of nanofluidic conversion. After correction, they turn to zero.

For excessive radii r_{etch} above ~35 nm in the regime C of Fig. 5b, the dr values grow slightly with r_{etch} for yet unclear reason. One might either speculate about some spatial relaxation of the enzyme layer with decreasing confinement, or about the possibility of multilayer enzyme coverage (if additional enzyme layers could stay permanently on top of the first one).

3.2. Biosensor calibration curves

Fig. 5 gives representative examples of the measured glucose sensor calibration curves (i.e., of the transmitted currents I(C) as a function of glucose concentration C, derived according to the nanofluidics conversion curve U_{osc}/U (r_{etch}) of Fig. 3c). For biosensors with very narrow pores (e.g. sensor #223, made from foil #6) with ~0.3 nm average track radius[5] (Fig. 5a), a bimodal behaviour shows up, consisting of a declining branch at very low glucose concentrations and an increasing one at very high glucose concentrations, joined by some broad intermediate region. The transition between the two branches of this

[5] According to nanofluidic evaluation.

bimodal calibration curve occurs at around 10^{-3} M for very narrow tracks (Fig. 5a), but increases towards $\sim 10^{-5}$ M for tracks with $\sim 3.5^{4}$ nm radius (for biosensor #219; not shown here). Simultaneously the two branches show less data scattering with increasing track radius. When increasing the track radius further, the decreasing branch vanishes rapidly and the increasing branch shows up with larger inclination up to the largest track radii recorded here (see as an example, sample #245 (side B of foil #15) with $r_{etch} \sim 15$ nm, Fig. 5b). For small currents (such as in Fig. 5a), the use of a 10 MΩ shunt gives pronouncedly sharper measuring results (concerning both the curve's slope and accuracy), whereas for larger sensor currents both the 1 and 10 MΩ shunt yield the same results.

The fact that even for unetched track sensors (i.e., $r_{etch} = 0$) a non-zero sensor response exists seems puzzling at the first moment. However, this and also the explication of the bimodal behaviour for sensors with very narrow pores is straightforward: Calibration curves with bimodal behaviour were only found for track radii < 16 nm, hence for tracks that accommodate only very few or no enzyme molecules on their walls. The nature of the declining branch at low C is explained thus: a) At analyte concentrations C below 1×10^{-7} M glucose, the observed current is a result of ultrapure water dissociation towards $[H^+]$ and $[OH^-]$ ions. When the concentration C of neutral glucose molecules is increased from 1×10^{-9} M to 1×10^{-6} M the relative concentration of $[H^+]$ and $[OH^-]$ ions from water decreases and so does the conductivity of the system. As compared with this current, the contribution of the ionized reaction products obtained from the few enzyme molecules in the tracks is negligible. Only when the glucose concentration approaches to 1×10^{-5} M, GOx becomes more active, and the system begins to accumulate charged products which rises the track's conductivity. Indeed, several literature reports [21–23] indicate an affinity constant, K_M, for GOx in the range from 1.9×10^{-5} M to 3.5×10^{-3} M. Therefore it is expected that the enzyme becomes more active when the glucose concentration approaches these values, which in turn results in a higher accumulation of reaction products. So there are two parameters, a higher product concentration and a higher enzyme activity which trigger the observed current increase between 10^{-5} and 1 M. b) When, after increasing the track radii r_{sensor} above 16 nm, continuous enzyme layers are formed on the track walls, the enzymatic reaction products dominate here from the beginning, and therefore only one rising calibration curve is found (as an example, see Fig. 5b). In conclusion, in track-based biosensors there exists a rather abrupt transition between structures clad with enzymes on their track walls (with $r_{sensor} \geq 16$ nm) which hence act as efficient biosensors, and structures with $r_{sensor} < 16$ nm with nanopores which are too small to accommodate a reasonable amount of enzymes and therefore are not useful for efficient biosensing.

3.3. The dependence of track-based biosensing on the track radius

In Fig. 6 we correlate (for all prepared glucose sensors with radii below ~25 nm) the recorded currents $I(r_{sensor})$ as a function of r_{sensor}, as determined via the nanofluidic oscilloscope's signal-to-radius conversion of Fig. 3c) for some selected glucose concentrations. Different regions show up, the most important one being that for r_{sensor} exceeding ~15 nm (region III), for which the sensor response is largest and constant (corresponding to the region B of Fig. 4b). Below that radius (corresponding to the region A of Fig. 4b) one recognizes a more or less constant but slightly fluctuating low current region from 0 to ~5 nm (I) and another rising one (II) which connects regions I and II.

Note that all curves in Fig. 6 are rather identical, indicating that the analyte concentration does not affect the sensor's behaviour above a characteristic threshold value around r_{thr} = 10–15 nm. (Note that dr (r_{etch}) in Fig. 4b follows a similar trend, insofar as beyond ~15 nm track radius dr is independent of r_{etch}). As below this threshold radius, no continuous enzyme layer deposition appears to be possible any longer due to excessive confinement, the sensor response decreases.

There are some tentative explanations for the emergence of the low-current region I such as a) enzyme bonding to the surface of the polymer foils or b) enzyme bonding to reactive sites on the latent track entrances, or c) some diffusion of EDC, S-NHS and GOx into surface-near regions, or d) their capillaric migration along crazes in the surface-near region and bonding there. We favor the last explanation, as the foils used by us (e.g., #6) had typical ages between half a decade and two decades, hence were already somewhat subject to degradation. According to the general understanding [24], typical degradation effects such as oxidation, hydrolisation, solar UV irradiation etc.) trigger stress between differently degraded polymer regions that relax by the formation of crazes (i.e., nano-cracks interconnected by fibrils). Eventually, the $I(r_{etch})$ curve slightly decreases from $r_{etch} = 0$ to ~3 nm, as suggested by the first one or two measuring points. At present we do not yet have, however, any satisfying explanation for such an effect; possibly this is only an artefact due to some slight data scattering.

A last point: Though the general trend of the curves in Region III indicates that they are parallel to each other, i.e. independent on track radius, one realizes some slightly correlated step-like jumps with increasing track radius at intermediate concentrations. As we can exclude any trivial reason (such as the erroneous assignment of wrong track radii or glucose concentrations, or variations of our hardware or software adjustment or of the used foil material or the lab temperature, or plotting errors), we might think at the possibility of slight abrupt relaxations of the polymeric track walls,[6] in dependence on the ambient parameters (such as the concentrations of the embedded solutions).

4. Summary and conclusions

In this work we wanted to examine the lower limits of swift heavy ion track-based biosensing, specifically for the "Product Enrichment" sensing strategy.

To check in how far tracks with very small radii are useful for track-based biosensors, we measured transmitted test currents as well across the as-etched tracks as across the final biosensors. Whereas for the conversion of the *as-etched* track signals to radii, it is obligatory to calculate these radii nanofluidically for the as-etched tracks, it was doubtful whether this is also required for biosensors, as in their cases surface charges are largely used up for enzyme bonding. Estimates show however, that also in their case nanofluidic corrections are useful.

At sufficiently high analyte concentrations ($> 10^{-6}$ M) and sufficiently high radii (> 15 nm), the biosensors exhibit their maximum sensitivity; here the currents always grow smoothly with the analyte concentration. Here, the sensors are also highly failure-tolerant as the measured sensor currents are independent of the individual track radii. A simple biosensor kinetics based on cylindrical etched tracks was established in the Supporting Information I to give predictions for these sensing conditions.

There exists, however, a limit for the analyte concentration, below which analyte-specific biosensing is impossible due to the inherent enzymatic kinetics. In this region, the sensor is just sensitive for any charge carrier. There exists also a lower limit for etched track radii (~3.5 nm) below which biosensors become useless for practical applications. In this region, a bimodal sensor signal emerges, one branch decreasing at lower analyte concentrations and another one increasing at higher concentrations. Whereas the first branch responds to any charge carrier, the second is analyte-specific, however with extremely poor sensitivity only.

A last point: It is known since long that very strong confinement – as

[6] In fact, similar (reversible) step-like changes have already been observed by us occasionally during slow track etching or during slow changes of the liquid inside the tracks (unpublished). These current jumps might either reflect abrupt changes of the polymer's nanometric structure as exposed to liquids at the etched track's inner wall surfaces, or they might indicate changes of the craze's configurations when exposed to different liquids. Detailed examinations of such effects are still missing.

given here in the tracks – decreases the diffusion of molecules embedded therein. As this would promote their enrichment, it was thought that this effect could be beneficial for track-based sensors. However, this is not the case; in the Supporting Information II we will show that this effect unfortunately cancels out.

Acknowledgements

D.F. is grateful to the Universidad Autónoma Metropolitana-Iztapalapa, Mexico City, for the guest professorship in the frame of the Cathedra "Alonso Fernandez." The project was supported by the Grant Agency of the Czech Republic (P108-12G-108) and the Nuclear Physics Institute, Řež near Prague. We are further obliged to Dr. P. Apel from JINR Dubna, Russia for providing us with the ion-irradiated polymer foil and to Prof. S. Cruz from UAM Mexico City, Mexico for many fruitful discussions. Finally we also want to thank the unknown reviewer for his excellent comments that helped us greatly to improve this work. Finally, we are very grateful for the excellent work of the anonymous reviewer which helped much to improve the quality of that paper.

Appendix A. Supplementary data

Supplementary data associated with this article can be found, in the online version, at http://dx.doi.org/10.1016/j.nimb.2018.02.010.

References

[1] D. Fink (Ed.), Fundamentals of Ion-Irradiated Polymers, Springer Series in Materials Science, Berlin, Heidelberg, 2004.
[2] D. Fink (Ed.), Transport Processes in Ion-irradiated Polymers, Springer Series in Materials Science, Berlin, Heidelberg, 2004.
[3] D. Fink, G. Muñoz Hernández, H. García Arellano, J. Vacík, V. Havranek, A. Kiv, L. Alfonta, Nuclear Track-Based Biosensing: An Overview, Radiat. Eff. Def. Solids 171 (2016) 173–183.
[4] D. Fink, J. Vacik, L. Alfonta, A. Kiv, Y. Mandabi, G. Muñoz H., Optimization of transport processes in etched track-based biosensors, Radiat. Eff. Def. Solids 167 (2012) 548–568.
[5] D. Fink, I. Klinkovich, O. Bukelman, R.S. Marks, A. Kiv, D. Fuks, W.R. Fahrner, L. Alfonta, Glucose determination using a re-usable enzyme-modified ion track membrane, Biosens. Bioelectron. 24 (2009) 2702–2706.
[6] D. Fink, G. Muñoz H., L. Alfonta,, Ion track-based urea sensing, Sens. Actuators B 156 (2011) 467–470.
[7] H. García Arellano, D. Fink, G. Muñoz H., J. Vacik, V. Hnatowicz, L. Alfonta, A nuclear track-based biosensor using the enzyme Laccase, Appl. Surf. Sci. 310 (2014) 66–76.
[8] D. Fink, G. Muñoz H., S.A. Cruz, H. García A., J. Vacik, V. Hnatowicz, A. Kiv, L. Alfonta, Ion track etching revisited: I. Correlations between track parameters in aged polymers, Nucl. Instr. Meth. B (2018) (accepted for publication).
[9] M. Daub, I. Enculescu, R. Neumann, R. Spohr, Ni nanowires electrodeposited in single ion track templates, J. Optoelectr. Adv. Mater. 7 (2005) 865–870.
[10] B. Schiedt, Characterization and application of ion track-etched nanopores (Ph.D. Thesis at the Ruperto-Carola), University of Heidelberg, Germany, 2007.
[11] H.J. Wirth, A. Gooley, Effects of particle porosity on the separation of larger molecules. Technical article by SGE Analytic Science, Australia (www.sge.com), http://www.sge.com/uploads/b8/4c/b84c77ffb452a93fe4d12d7401dfa60b/TA-0136-H.pdf.
[12] L. Bocquet, E. Charlaix, Nanofluidics, from bulk to interface, in: A.Van den Berg, H. Craighead, P. Yand (Eds.), From Microfluidic Application to Nanofluidic Phenomena Issue: Reviewing the Latest Advances in Microfluidic and Nanofluidic Research, Chemical Society Reviews, vol. 39, 2010, pp. 1073–1095.
[13] S. Prakash, M. Pinti, B. Bhushan, Scaling Theory, fabrication and applications of microfluidic and nanofluidic biosensors, Phil. Trans. R. Soc. A 370 (2017) 2269–2303.
[14] D.G. Haywood, A. Saha-Shah, L.A. Baker, S.C. Jacobson, Fundamental studies of nanofluidics: nanopores, nanochannels, and nanopipets analytical chemistry, Anal. Chem. 87 (2015) 172–187.
[15] W. Sparreboom, A. van den Berg, J.C.T. Eijkel, Transport in nanofluidic systems: a review of theory and applications, New J. Phys. 12 (2010) 015004 (23pp).
[16] D. Stein, M. Kruithof, C. Dekker, Surface-charge-governed ion transport in nanofluidic channels, Phys. Rev. Lett. 93 (2004) 035901-1 to 035901-4.
[17] K. Kant, C. Priest, J.G. Shapter, D. Losic, The influence of nanopore dimensions on the electrochemical properties of nanopore arrays studied by impendance spectroscopy, Sensors 14 (2014) 21316–21328.
[18] J.E. Hall, Access resistance of a small circular pore, J. General Phys. 66 (1975) 531–532.
[19] B. Hille, Pharmacological modifications of the sodium channels of frog nerve, J. Gen. Physiol. 51 (1968) 199–219.
[20] C. Lee, L. Joly, A. Siria, A.-L. Biance, R. Fulcrand, L. Bocquet, Large apparent electric size of solid-state nanopores due to spatially extended surface conduction, Nano Lett. 12 (2012) 4037–4044.
[21] A. Seehuber, R. Dahint, Conformation and activity of glucose oxidase on homogeneously coated and nanostructured surfaces, J. Phys. Chem. B 117 (2013) 6980–6989.
[22] Y.K. Cho, J.E. Bailey, Immobilization of enzymes on activated carbon: Properties of immobilized glucoamylase, glucose oxidase, and gluconolactone, Biotechnol. Bioeng. 20 (1978) 1651–1665.
[23] G. Wohlfahrt, S. Trivić, J. Zeremski, D. Pericin, V. Leskovac, The chemical mechanism of action of glucose oxidase from Aspergillus niger, Mol. Cell Biochem. 260 (2004) 69–83.
[24] A. Mikdam, X. Colin, G. Minard, N. Billon, R. Maurin, A kinetic model for predicting the oxidative degradation of additive free polyethylene in bleach disinfected water, Polymer Degrad. Stab. 146 (2017) 78–94.